International Journal of Applied Mathematics

Volume 34 No. 3 2021, 555-574
ISSN: 1311-1728 (printed version); ISSN: 1314-8060 (on-line version)
doi: http://dx.doi.org/10.12732/ijam.v34i3.10

AN ALTERNATIVE SMOOTHNESS MEASURE FORMULATION OF TARGETED ENO SCHEMES FOR COMPRESSIBLE FLOW SIMULATION

Indra Wibisono[1], Engkos A. Kosasih[2], Yanuar[3] §

[1,2,3] Department of Mechanical Engineering
Universitas Indonesia
16424 Depok, Jawa Barat, INDONESIA

Abstract: In this paper, we propose an alternative smoothness measure formulation using power $p = 2$ of ratio $\frac{\tau_K}{\beta_{k,r}}$ for TENO schemes. The spectral properties of the alternative scheme suggest comparable dissipation and dispersion with the original five-point TENO schemes. The advantage of this alternative scheme is a more distinct scale separation at a high wavenumber. Our numerical experiments reveal that the resolution in one-dimensional problems is quite similar to the original five-point TENO scheme. Despite this, the resolution in two-dimensional problems gives an alternative fine-scale structure.

AMS Subject Classification: 65M08, 35L65
Key Words: high-order schemes; low-dissipation schemes; TENO; shock-capturing schemes; finite-volume method

1. Introduction

In recent decades, studies on high-order schemes for computational physics have been yielding remarkable results. These schemes have been designed to work efficiently within a multiscale structure and also to cope with discontinuous problems [1]. Moreover, due to the independence of the schemes from the problem set, they can have broad implementations, for example, for computational

Received: December 4, 2020

§Correspondence author

fluid dynamics, solid mechanics, and acoustics. The development of high-order schemes is also compatible with the available hardware today.

The origin of one of the most successful high-order schemes, which is known as the weighted essentially non-oscillatory (WENO) scheme, has been discussed in classical papers [1, 2, 3]. The capacity of WENO to resolve discontinuities alongside its essentially non-oscillatory (ENO) properties, makes it a reliable high-order numerical scheme, the essential factor of WENO that has been the focus of much research. The improvements have been yielding more accurate performance [4, 5, 6], computational efficiency [7, 8, 9], and robustness [10, 11, 12]. Most of WENO's performance depends on the construction of nonlinear weights and their smoothness measurement. The WENO-Z scheme of Borges et al. [5] resolve the convergence near critical points by measuring full-point stencil smoothness, commonly known as the global reference smoothness indicator; it is also assigned to a new technique of constructing the nonlinear weights. Later, Hu et al. [13] developed a sixth-order WENO central-upwind (WENO-CU6) scheme. New weighting strategy of WENO-CU6 allowed a smooth transition between central and upwind schemes, yielding a less-dissipative scheme. Subsequently, Hu et al. [14] modified WENO-CU6 for implicit large-eddy simulations (ILES) by setting a higher integer power to WENO weights. As a result, their proposed scheme provided better scale-separations but generated spurious waves at a particular wavenumber [15].

In their design of targeted ENO (TENO) schemes, Fu et al. [16] proposed a new perspective of constructing nonlinear weights. TENO follows the ENO-like stencil selections, meaning the complete removal of the discontinuous stencil with a specific strength. The nature of TENO is different from the classical WENO scheme; for example, fifth-order TENO schemes can automatically degenerate to third-order ones when crossing discontinuity. This new approach ameliorated scale-separations by isolating discontinuity [14]. Through the analysis of approximate dispersion relation (ADR) (see Jia et al. [17]), TENO schemes can recover linear background schemes in wider wavenumbers compared with classical WENO schemes. As a result, TENO schemes yield better dispersion with low numerical dissipation.

TENO schemes of Fu et al. [16] adopted the WENO-Z smoothness measure when the power of $\frac{\tau_K}{\beta_{k,r}}$ was set to 1. WENO-Z with a high power of $\frac{\tau_K}{\beta_{k,r}}$, produces dissipative results in the discontinuous region. However, the results are different if it is applied to TENO schemes, mainly due to the indirect use of measured smoothness. In this paper, we propose an alternative formulation using a different power of proportion $\frac{\tau_K}{\beta_{k,r}}$ for TENO schemes. We demonstrate the capability of the alternative scheme to solve Euler equations of gas dynam-

ics. Furthermore, we compare the results with TENO schemes of Fu et al. [16] in terms of numerical accuracy and fine-scale resolutions.

The remainder of this paper is organized as follows. In Section 2, we review WENO-Z and TENO schemes. The alternative smoothness measurement of the TENO scheme and the analysis of approximate dispersion relation are discussed in Section 3. Several tests in one- and two-dimensional problems are conducted and presented in Section 4. Finally, the conclusions are provided in Section 5.

2. Review of WENO-Z and TENO schemes

First, we consider the hyperbolic conservation law

$$\frac{\partial u}{\partial t} + \frac{\partial}{\partial x} f(u) = 0, \tag{1}$$

where u denotes the conserved variable, and f denotes the physical flux. Consider computational cell $I_i = [x_{i-1/2}, x_{i+1/2}]$ and uniform grid spacing Δx. The semi-discrete form of (1) by means of the finite-volume method is represented as

$$\frac{d\bar{u}_i(t)}{dt} \simeq -\frac{1}{\Delta x}\left(\hat{f}_{i+\frac{1}{2}} - \hat{f}_{i-\frac{1}{2}}\right), \tag{2}$$

where

$$\bar{u} = \frac{1}{\Delta x}\int_{I_i} u(\xi, t)d\xi \tag{3}$$

and $\hat{f}_{i\pm1/2}$ denotes the numerical flux at cell interface $x_{i\pm1/2}$. Flux $\hat{f}_{i+1/2}$ is evaluated by the exact or approximate Riemann solver

$$\hat{f}_{i+1/2} = H(u^-_{i+\frac{1}{2}}, u^+_{i+\frac{1}{2}}), \tag{4}$$

where $u^-_{i+1/2}$ and $u^+_{i+1/2}$ denote the left and right interpolated values of the conserved variable at cell interface $x_{i+1/2}$. The interpolated values are evaluated by WENO/TENO schemes to achieve high-order accuracy in the smooth region and give non-oscillatory behavior.

2.1. Fifth-order WENO-Z schemes

WENO schemes achieve high-order approximation by combining the lower order polynomials. In the fifth-order version ($r = 3$), three three-point stencils

$\{S_0, S_1, S_2\}$ are used to construct the quadratic polynomial; they are then combined into the fifth-order polynomial in the larger stencil (i.e., S^5). The value of $u_{i+1/2}$ in terms of cell-averaged quantity can be written as

$$u^{(0)}_{i+\frac{1}{2}} = \tfrac{1}{6}\left(2\bar{u}_{i-2} - 7\bar{u}_{i-1} + 11\bar{u}_i\right), \tag{5a}$$

$$u^{(1)}_{i+\frac{1}{2}} = \tfrac{1}{6}\left(-\bar{u}_{i-1} + 5\bar{u}_i + 2\bar{u}_{i+1}\right), \tag{5b}$$

$$u^{(2)}_{i+\frac{1}{2}} = \tfrac{1}{6}\left(2\bar{u}_i + 7\bar{u}_{i+1} - \bar{u}_{i+2}\right). \tag{5c}$$

The fifth-order interpolation can be written as

$$u^{-}_{i+\frac{1}{2}} = \sum_{k=0}^{2} w_k u^{(k)}_{i+\frac{1}{2}}. \tag{6}$$

Given by Borges et al. [5], nonlinear weight w_k is defined as

$$w_k = \frac{\alpha_k}{\sum \alpha_k}, \quad \alpha_k = d_k\left(1 + \left(\frac{\tau_K}{\beta_{k,r} + \varepsilon}\right)^p\right), \tag{7}$$

where $\beta_{k,r}$ denotes the smoothness indicator; τ_K $(K = 2r-1)$ denotes the full-point smoothness indicator, known as the global reference smoothness indicator; and $\varepsilon = 10^{-40}$ denotes the sensitivity parameter to hold the denominator down to zero. Optimal weights d_k is $\left\{\frac{1}{10}, \frac{6}{10}, \frac{3}{10}\right\}$, so they achieve fifth-order accuracy for sufficiently smooth functions. Typically, the power parameter of WENO-Z schemes was set to $p = 1$. According to Borges et al. [5], an increase in the power ratio of $\frac{\tau_K}{\beta_{k,r}}$ would lessen the discontinuous stencil contribution, and yield more dissipative results. The smoothness indicator definition is given by

$$\beta_{k,r} = \sum_{l=1}^{r-1} \int_{I_i} \Delta x^{2l-1}\left(\frac{\partial^l}{\partial x^l} u^{(k)}(x)\right)^2 dx. \tag{8}$$

In the actual implementation, the smoothness indicators are expressed in terms of the cell-averaged value of the conserved quantity, as follows:

$$\beta_{0,3} = \frac{1}{4}(\bar{u}_{i-2} - 4\bar{u}_{i-1} + 3\bar{u}_i)^2 + \frac{13}{12}(\bar{u}_{i-2} - 2\bar{u}_{i-1} + \bar{u}_i)^2, \tag{9a}$$

$$\beta_{1,3} = \frac{1}{4}(3\bar{u}_{i-1} - \bar{u}_{i+1})^2 + \frac{13}{12}(\bar{u}_{i-1} - 2\bar{u}_i + \bar{u}_{i+1})^2, \tag{9b}$$

$$\beta_{2,3} = \frac{1}{4}(3\bar{u}_i - 4\bar{u}_{i+1} + \bar{u}_{i+2})^2 + \frac{13}{12}(\bar{u}_i - 2\bar{u}_{i+1} + \bar{u}_{i+2})^2. \tag{9c}$$

The global reference smoothness indicator is given by

$$\tau_5 = |\beta_{0,3} - \beta_{2,3}| = \mathrm{O}\left(\Delta x^5\right). \tag{10}$$

In the smooth solution, nonlinear weight satisfies $w_k = d_k + \mathrm{O}\left(\Delta x^3\right)$ when the critical point does not emerge. Even if the critical point is present, WENO-Z still yield better accuracy than the classical WENO-JS scheme [18].

2.2. Fifth-order TENO schemes

High-order TENO reconstruction uses a different approach to the construction of their nonlinear weights. The schemes do not directly use the measured smoothness but assign it to isolate the stencil that has a particular strength of discontinuity from being used in the reconstruction. When crossing a discontinuity, the schemes automatically degenerate into lower order. This approach yields more robust, accurate, and improve the scale-separation property. Drawing on Borges et al. [5] and Hu et al. [14], the TENO scheme smoothness measurement is formulated as follows:

$$\gamma_k = \left(C + \frac{\tau_K}{\beta_{k,r} + \varepsilon}\right)^q. \tag{11}$$

The integer power is set to $q = 6$, and the constant parameter is set to $C = 1$. TENO schemes have weaker conditions for the order of $\frac{\tau_K}{\beta_{k,r}}$ [16], where it should satisfy

$$\frac{\tau_K}{\beta_{k,r}} = \mathrm{O}\left(\Delta x^s\right), \quad s > 0. \tag{12}$$

Sixth-order τ_K is suitable for TENO-family schemes and prefered to achieve strong scale separation [19]. Thus, sixth-order τ_K can be constructed:

$$\tau_K = \left|\beta_K - \frac{1}{6}\left(\beta_{0,3} + \beta_{2,3} + 4\beta_{1,3}\right)\right| = \mathrm{O}\left(\Delta x^6\right). \tag{13}$$

Then, the measured smoothness is normalized as follows:

$$\vartheta_k = \frac{\gamma_k}{\sum \gamma_k}. \tag{14}$$

The use of a cutoff function yields the following:

$$\upsilon_k = \begin{cases} 0, & \vartheta_k < C_T, \\ 1, & \text{otherwise}, \end{cases} \tag{15}$$

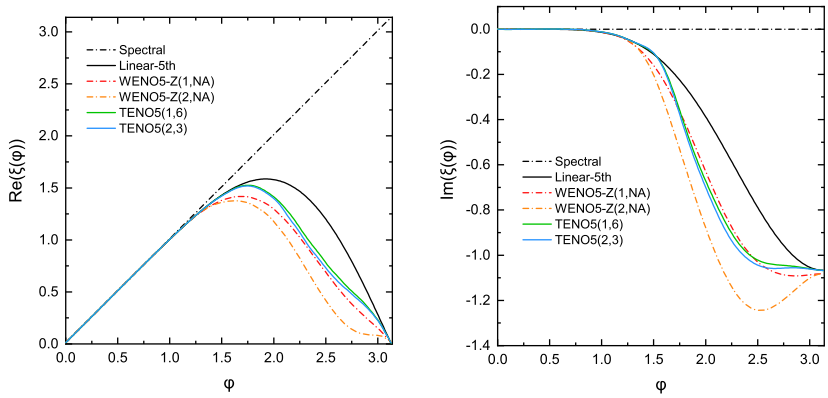

Figure 1: Approximate dispersion (left) and dissipation (right) of WENO5-Z and TENO5 schemes.

the normalized smoothness is eliminated if it exceeds the specific threshold of C_T. The final assembled optimal weights are formulated as

$$w_k = \frac{d_k \upsilon_k}{\sum d_k \upsilon_k}, \tag{16}$$

and the final interpolation of the conserved variable at cell interface is performed using Eq. (6).

3. An alternative smoothness measure formulation of TENO schemes

Motivated by Borges et al.'s [5] and Fu et al.'s [16] works, we introduce an alternative smoothness measure formulation for TENO schemes, as follows:

$$\gamma_k = \left(C + \left(\frac{\tau_K}{\beta_{k,r} + \varepsilon} \right)^p \right)^q. \tag{17}$$

We set $C = 1$, $p = 2$, $q = 3$, and sensitivity parameter $\varepsilon = \Delta x^4$ (refer to Table 3 in Don et al. [20]). For convenience, we denote the power parameters by "scheme"(p, q), following notation of Eq. (17); however, power parameter q is not applicable to WENO-Z. Thus, we set $C_T = 10^{-5}$ for TENO schemes.

Figure 1 presents the spectral property of fifth-order WENO-Z and TENO schemes using approximate dispersion relation (ADR) analysis (consult Jia et

al. [17] and Pirozzoli et al. [21] for more details). The proposed TENO5(2,3) scheme yields better spectral property from both WENO5-Z(1,NA) and WENO5-Z(2,NA) in almost the entire wavenumber. While TENO5(2,3) spectral property is comparable with the result of TENO5(1,6), the only difference is at the high wavenumber.

4. Numerical results

In this section, we consider the two-dimensional Euler equations:

$$\mathbf{U}_t + \mathbf{F}_x + \mathbf{G}_y = 0, \tag{18}$$

where the vector of conservative variables $\mathbf{U} = (\rho, \rho u, \rho v, \rho E)^T$. The corresponding fluxes are

$$\mathbf{F} = \left[\rho u, \rho u^2 + p, \rho uv, (E+p)\, u\right]^T$$

and

$$\mathbf{G} = \left[\rho v, \rho vu, \rho v^2 + p, (E+p)\, v\right]^T$$

for fluxes in x- and y-directions, respectively. Also, ρ, p, u, v and E represent density, pressure, velocity in the x-direction, velocity in the y-direction, and total energy, respectively. The equation of state (EOS) is $E = p/(\gamma - 1) + \frac{1}{2}\rho\left(u^2 + v^2\right)$, where γ is the specific heat ratio. In this paper, $\gamma = 1.4$ unless stated otherwise. Flux integration over cell interface is approximated by a four-point Gauss-Legendre quadrature to ensure that the scheme achieves maximum order in multidimensional reconstruction [22]. The characteristic transformation is carried out to minimize spurious oscillation. Flux calculation is performed using the Harten–Lax–van Leer contact (HLLC) approximate Riemann solver [23]. The resulting time-dependent ordinary differential equations (ODEs) after spatial discretization are integrated by third-order total variation diminishing (TVD) Runge-Kutta method [24], with $CFL = 0.4$ for all computations.

4.1. One-dimensional accuracy test

We first consider the one-dimensional Euler equation of Eq. (18) by neglecting the y-component flow. The initial condition is $(\rho, u, p) = (1 + 0.2\sin(\pi x), 1, 1)$, which evolves up to $t = 2$. The computational domain is $[-2, 2]$, and timestep Δt is scaled down by $\Delta x^{5/3}$.

Table 1: Numerical error and convergence order of tested schemes in the one-dimensional smooth problem.

N	WENO5-Z(1,NA)		TENO5(1,6)		TENO5(2,3)	
	L1 Error	Order	L1 Error	Order	L1 Error	Order
10	3.08E-02		2.79E-02		2.79E-02	
20	1.51E-03	4.35	1.20E-03	4.54	1.20E-03	4.54
40	4.33E-05	5.12	4.06E-05	4.89	4.06E-05	4.89
80	1.30E-06	5.06	1.29E-06	4.97	1.29E-06	4.97
160	4.06E-08	5.00	4.06E-08	4.99	4.06E-08	4.99
320	1.27E-09	5.00	1.27E-09	5.00	1.27E-09	5.00

Table 1 presents the L_1 error and the convergence order for density. All tested schemes converge toward the desired order of accuracy, whereas TENO5(1,6) and TENO5(2,3) yield a smaller dissipation than WENO5-Z(1,NA) in the coarse grid.

4.2. One-dimensional shock tube problem

The initial condition of the shock tube problem is given by

$$(\rho, u, p) = \begin{cases} (1, 0, 1), & 0 \le x < 0.5, \\ (0.125, 0, 0.1), & 0.5 \le x \le 1, \end{cases} \tag{19}$$

and the simulations march up to time $t = 0.2$.

Figure 2 presents the computed density and velocity profiles at the final time using the $N = 100$ cells. All the schemes provide comparable results for this shock tube problem.

4.3. Interacting blast wave

We consider the interacting blast wave problem with the following initial conditions

$$(\rho, u, p) = \begin{cases} (1, 0, 1000)\,, & 0 \le x < 0.1, \\ (1, 0, 0.1)\,, & 0.1 \le x < 0.9, \\ (1, 0, 100)\,, & 0.9 \le x \le 1, \end{cases} \tag{20}$$

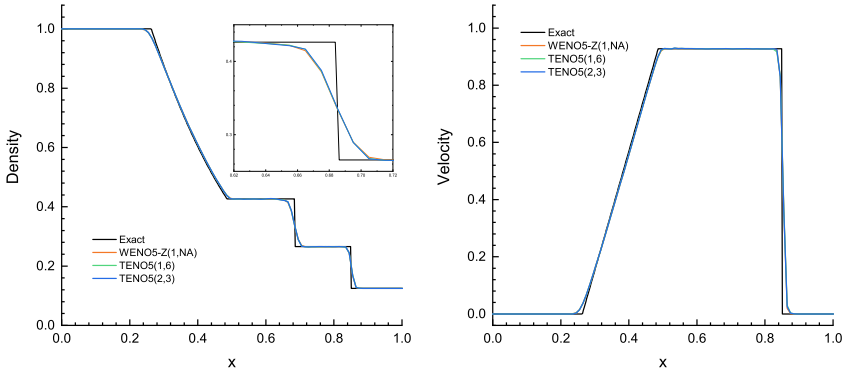

Figure 2: Density profile (left) and velocity profile (right) of Sod's shock tube problem at $t = 0.2$.

imposed with reflective boundary conditions on either side. The final time is $t = 0.038$ and is discretized using the $N = 400$ cells. The "exact" solution is computed employing 2000 cells using the WENO-JS scheme.

The density profile at the final time is presented in Figure 3. Compared with WENO5-Z(1,NA), both TENO5 schemes improve the peak value and the valley at $x = 0.78$ and $x = 0.75$, respectively, whereas the alternative scheme TENO5(2,3) yields almost the same result as TENO5(1,6).

4.4. Shock density wave interaction

The interaction of the sine wave with the Mach 3 wave generates discontinuity along with fine-scale structures. The initial condition of the shock density wave interaction is given by

$$(\rho, u, p) = \begin{cases} (3.857143, 2.629369, 10.333333)\,, & x < -4, \\ (1 + \varepsilon \sin(5x)\,, 0, 1)\,, & x \geq -4, \end{cases} \tag{21}$$

with $\varepsilon = 0.2$. The domain is $[-5, 5]$, and the number of cells is set to $N = 300$. The final time is set to $t = 1.8$.

Figure 4 presents the density profile computed by three different schemes and an "exact" solution computed employing 2000 points using WENO-JS. Compared to WENO5-Z(1,NA), all of the TENO5 schemes improve the wave amplitude due to better scale-separation properties. TENO5(2,3) presents almost identical results with TENO5(1,6).

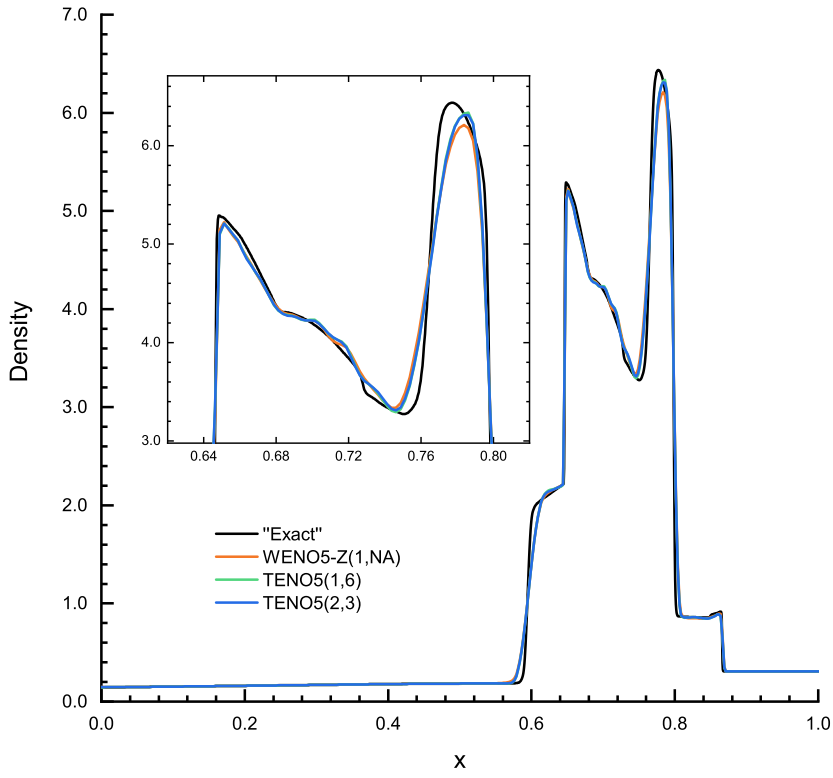

Figure 3: Solution of the interacting blast wave problem: density profile at $t = 0.038$.

4.5. Two-dimensional accuracy test

The initial condition for the two-dimensional accuracy test is

$$(\rho, u, v, p) = (1 + 0.2\sin(\pi x), 0.7, 0.3, 1),$$

and evolves up to $t = 2$. The computational domain is $[-2, 2] \times [-2, 2]$, and as mentioned before, timestep Δt is scaled down.

Table 2 presents the L_1 error and the convergence order for density. All tested schemes converge toward the desired order of accuracy, whereas TENO5(1,6) and TENO5(2,3) yield smaller dissipation than WENO5-Z(1,NA).

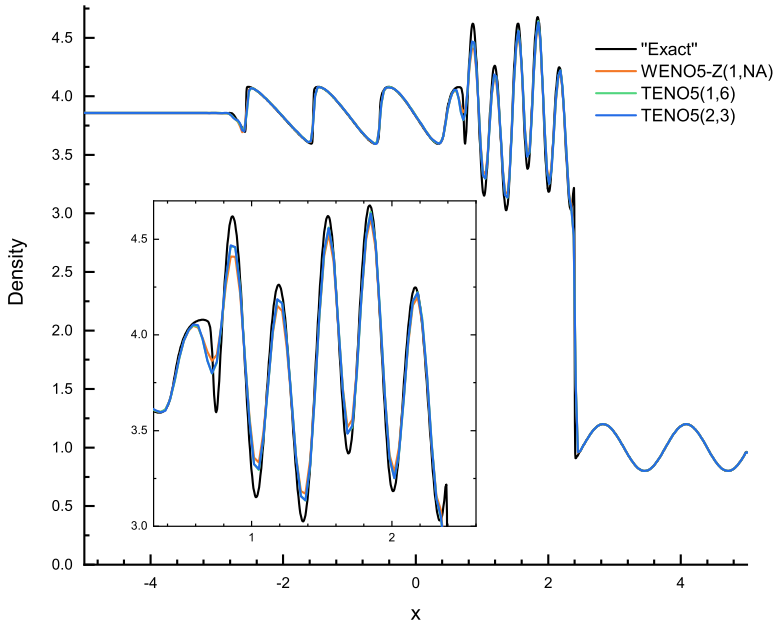

Figure 4: Solution of shock density wave interaction: density profile at $t = 1.8$.

4.6. Two-dimensional Riemann problem

We consider the third configuration of Lax et al.[25] with the initial condition set as

$$(\rho, u, v, p) = \begin{cases} (1.5, 0, 0, 1.5)\,, & \text{if } x > 0.5, y > 0.5, \\ (0.5323, 1.206, 0, 0.3)\,, & \text{if } x < 0.5, y > 0.5, \\ (0.138, 1.206, 1.206, 0.029)\,, & \text{if } x < 0.5, y < 0.5, \\ (0.5323, 0, 1.206, 0.3)\,, & \text{otherwise.} \end{cases} \tag{22}$$

The domain is $[0, 1] \times [0, 1]$, and the number of cells is set to 720×720.

Figure 5 presents the results of the two-dimensional Riemann problem at $t = 0.23$. The result are quite similar. However, in some areas, TENO schemes yield better secondary scales than the WENO5-Z(1,NA) scheme. TENO5(2,3)

Table 2: Numerical error and convergence order of tested schemes in the two-dimensional smooth problem.

N	WENO5-Z(1,NA)		TENO5(1,6)		TENO5(2,3)	
	L1 Error	Order	L1 Error	Order	L1 Error	Order
10	2.92E-02		2.65E-02		2.65E-02	
20	1.52E-03	4.26	1.22E-03	4.43	1.22E-03	4.43
40	4.22E-05	5.17	3.96E-05	4.95	3.96E-05	4.95
80	1.21E-06	5.13	1.20E-06	5.04	1.20E-06	5.04
160	3.49E-08	5.11	3.49E-08	5.10	3.49E-08	5.10
320	1.04E-09	5.07	1.04E-09	5.07	1.04E-09	5.07

indicates slightly different flow structures than TENO5(1,6), for example, at the center of the domain. We further consider the 17th configuration of two-dimensional Riemann problem [25], with the following initial conditions:

$$(\rho, u, v, p) = \begin{cases} (1.0, 0, -0.4, 1.0)\,, & \text{if } x > 0.5, y > 0.5, \\ (2.0, 0.0, -0.3, 1.0)\,, & \text{if } x < 0.5, y > 0.5, \\ (1.0625, 0, 0.2145, 0.4)\,, & \text{if } x < 0.5, y < 0.5, \\ (0.5197, 0, -1.1259, 0.4)\,, & \text{if } x > 0.5, y < 0.5. \end{cases} \tag{23}$$

We set the domain and the number of cells as the previous third configuration of the two-dimensional Riemann problem simulation, with system evolving up to $t = 0.3$.

As presented in Figure 6, TENO schemes give superior small-scale resolution over WENO5-Z(1,NA). TENO5(2,3) indicates slightly different flow structures than TENO5(1,6).

4.7. Rayleigh-Taylor instabilities

The problem has the following initial conditions:

$$(\rho, u, v, p) = \begin{cases} (2, 0, -0.025c\cos(8\pi x)\,, 1 + 2y)\,, & 0 \le y < 1/2 \\ (1, 0, -0.025c\cos(8\pi x)\,, y + 3/2)\,, & 1/2 \le y \le 1, \end{cases} \tag{24}$$

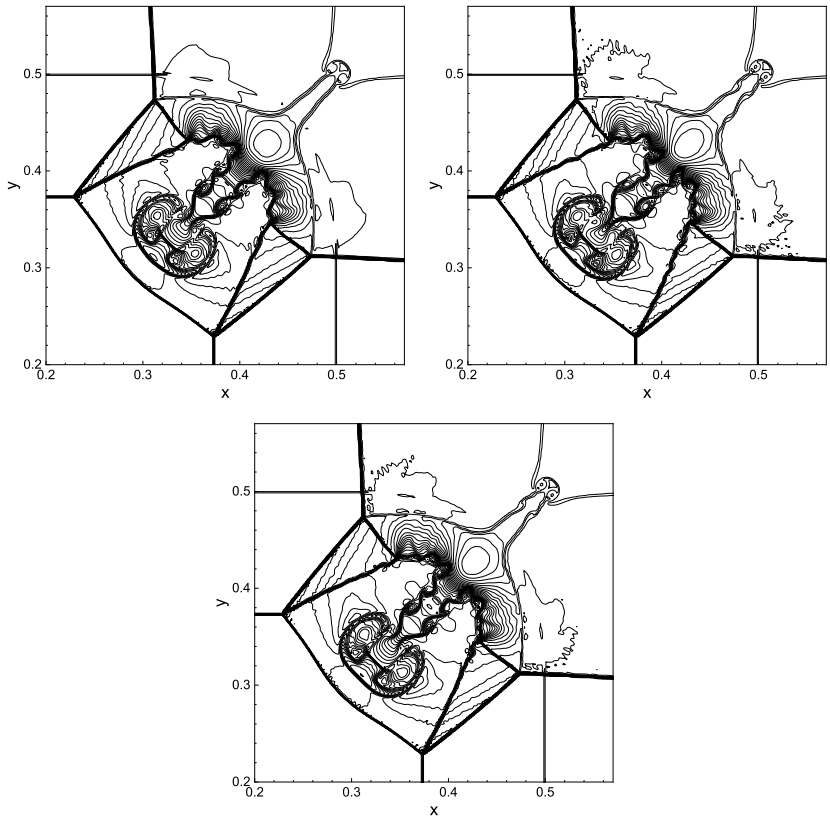

Figure 5: Density contour of the two-dimensional Riemann problem of third configuration at $t = 0.23$. Top left: WENO5-Z(1,NA), top right: TENO5(1,6), bottom: TENO5(2,3).

where c denotes the sound speed with a specific heat ratio of $\gamma = \frac{5}{3}$. The computational domain is $[0, 0.25] \times [0, 1]$. With the reflective wall boundary conditions in the left and right domains, the upper boundary is enforced to $(\rho, u, v, p) = (1, 0, 0, 2.5)$, and the bottom boundary is enforced to $(\rho, u, v, p) = (2, 0, 0, 1)$. The source terms for the third and fourth equations of Eq. (18) are set to ρ and ρv respectively. The solution is extractedn at a resolution of 128×512 at the final time $t = 1.95$.

As presented in Figure 7, contrary to TENO schemes, WENO5-Z(1,NA) preserves the flow symmetry. In the overall solution, all TENO schemes yield

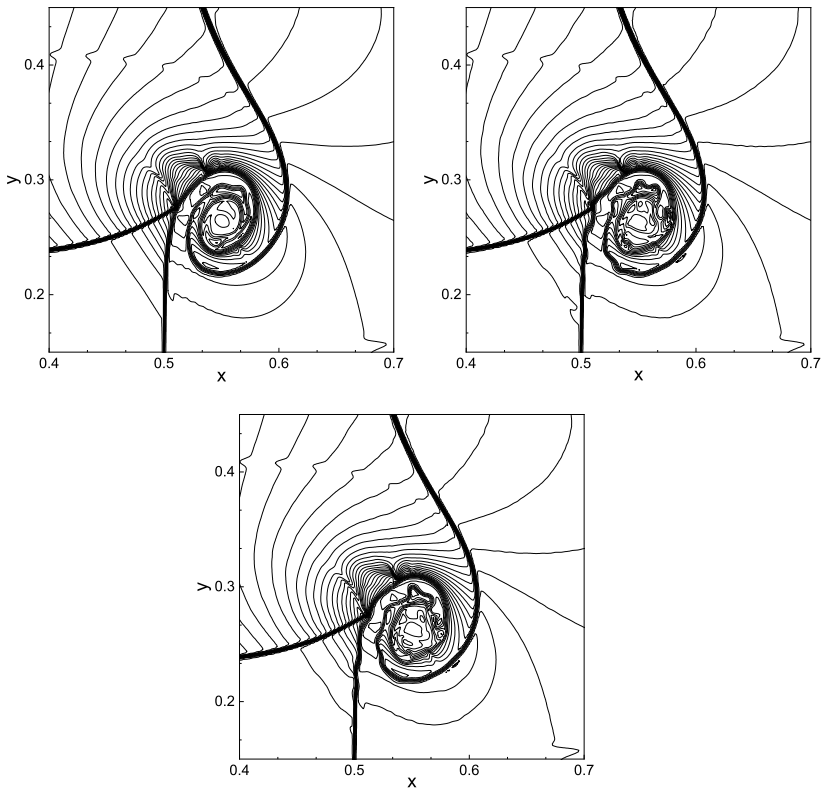

Figure 6: Density contour of the two-dimensional Riemann problem of the 17th configuration at $t = 0.3$. Top left: WENO5-Z(1,NA), top right: TENO5(1,6), bottom: TENO5(2,3).

better fine-scale structures than the WENO5-Z(1,NA). The cap part solution of TENO5(2,3) gives considerably more symmetrical results than TENO5(1,6). The resolved vortical structure is interpreted differently in TENO5(1,6) and TENO5(2,3), although it has almost the same quantity.

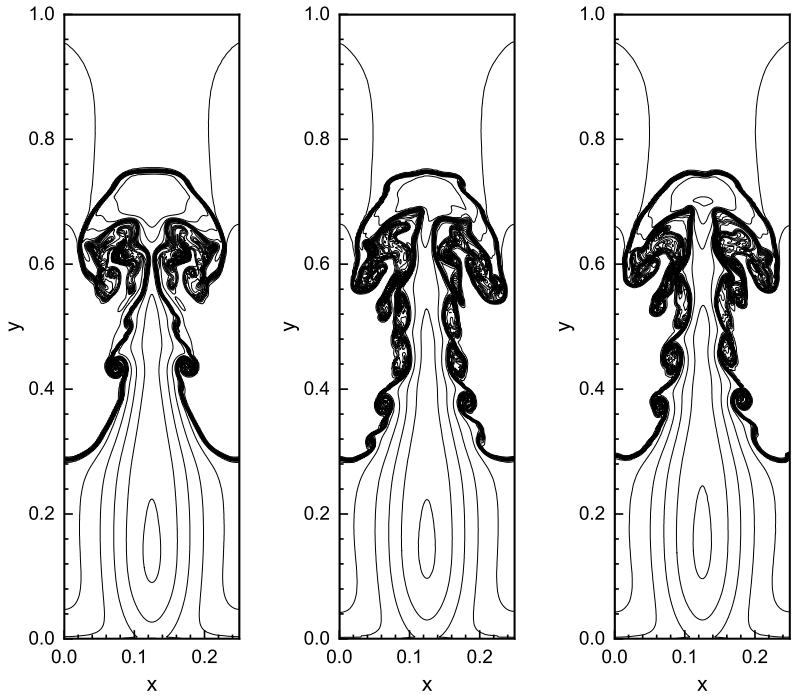

Figure 7: Density contour of Rayleigh-Taylor instability at $t = 1.95$. Left: WENO5-Z(1,NA), middle: TENO5(1,6), right: TENO5(2,3).

4.8. Double Mach reflection

Finally, we consider the double Mach reflection problem [26] with the following initial conditions:

$$(\rho, u, v, p) = \begin{cases} (1.4, 0, 0, 1)\,, & \text{if } x < \frac{1}{6} + \frac{y}{\sqrt{3}}, \\ (8, 7.145, -4.125, 116.8333)\,, & \text{otherwise.} \end{cases} \tag{25}$$

Mach 10 shock with an incident angle of 60° to the x-axis, initially at $x = \frac{1}{6}$, moves along the x-direction. The computational domain is set to $[0, 4] \times [0, 1]$ and discretized using the 240×960 cells. The bottom boundary at $0 < x < \frac{1}{6}$ is set to the exact post-shock condition and reflective wall boundary condition for $\frac{1}{6} < x < 4$. Then, the system evolves up to $t = 0.2$.

As presented in Figure 8, all TENO schemes develop a finer flow struc-

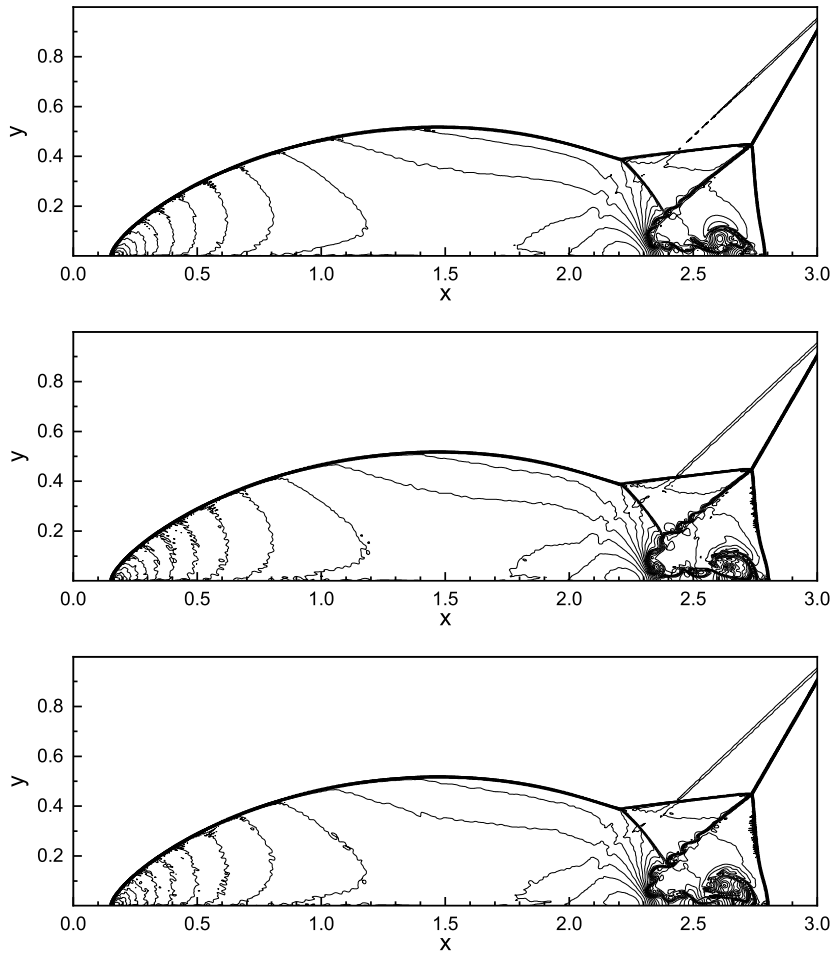

Figure 8: Density contour of double Mach reflection at $t = 0.2$. Top: WENO5-Z(1,NA), middle: TENO5(1,6), bottom: TENO5(2,3).

ture than WENO5-Z(1,NA) at the primary slip line. The use of the Gaussian quadrature for flux integration suggests a better resolution at the jet of the primary slip line compared with the result of Fu et al. [27] using the mid-point rule. Again, compared with TENO5(1,6) we notice a different interpretation of the fine-scale resolution of TENO5(2,3).

5. Conclusions

In this paper, we proposed a different smoothness measure formulation for TENO schemes using the basis of WENO-Z schemes by $p = 2$ of ratio $\frac{\tau_K}{\beta_{k,r}}$. Moreover, we conducted extensive numerical experiments in one- and two-dimensional problems. The resolution in one-dimensional problems is quite similar to the original five-point TENO5(1,6) scheme. However, the resolution in two-dimensional problems gives an alternative fine-scale structure. The advantage of the TENO5(2,3) scheme is a more distinct scale separation at high wavenumber, despite the dissipation being slightly larger than TENO5(1,6).

Acknowledgement

This research was fully supported by Hibah Publikasi Terindeks Internasional (PUTI) Q2 2020 of Universitas Indonesia, Grant Number NKB-1749/UN2.RST/HKP.05.00/2020.

References

[1] G.-S. Jiang, C.-W. Shu, Efficient implementation of weighted ENO schemes, *J. of Comput. Physics*, **126**, No 1 (1996), 202-228; doi: 10.1006/jcph.1996.0130.

[2] A. Harten, B. Engquist, S. Osher, S.R. Chakravarthy, Uniformly high order accurate essentially non-oscillatory schemes, III, *J. of Comput. Physics*, **71**, No 2 (1987), 231-303; doi: 10.1016/0021-9991(87)90031-3.

[3] X.-D. Liu, S. Osher, T. Chan, Weighted essentially non-oscillatory schemes, *J. of Comput. Physics*, **115**, No 1 (1994), 200-212; doi: 10.1006/jcph.1994.1187.

[4] A.K. Henrick, T.D. Aslam, J.M. Powers, Mapped weighted essentially non-oscillatory schemes: Achieving optimal order near critical points, *J. of Comput. Physics*, **207**, No 2 (2005), 542-567; doi: 10.1016/j.jcp.2005.01.023.

[5] R. Borges, M. Carmona, B. Costa, W.S. Don, An improved weighted essentially non-oscillatory scheme for hyperbolic conservation laws, *J. of Comput. Physics*, **227**, No 6 (2008), 3191-3211; doi: 10.1016/j.jcp.2007.11.038.

[6] Y. Ha, C.H. Kim, Y.J. Lee, J. Yoon, An improved weighted essentially non-oscillatory scheme with a new smoothness indicator, *J. of Comput. Physics*, **232**, No 1 (2013), 68-86; doi: https://doi.org/10.1016/j.jcp.2012.06.016.

[7] Z. Zhao, J. Zhu, Y. Chen, J. Qiu, A new hybrid WENO scheme for hyperbolic conservation laws, *Computers & Fluids*, **179** (2019), 422-436; doi: 10.1016/j.compfluid.2018.10.024.

[8] J. Peng, C. Zhai, G. Ni, H. Yong, Y. Shen, An adaptive characteristic-wise reconstruction WENO-Z scheme for gas dynamic Euler equations, *Computers & Fluids*, **179** (2019), 34-51; doi: 10.1016/j.compfluid.2018.08.008.

[9] R. Kumar. P. Chandrashekar, Efficient seventh order WENO schemes of adaptive order for hyperbolic conservation laws, *Computers & Fluids*, **190** (2019), 49-76; doi: 10.1016/j.compfluid.2019.06.003.

[10] J. Shi, C. Hu, C.-W. Shu, A Technique of Treating Negative Weights in WENO Schemes, *J. of Comput. Physics*, **175**, No 1 (2002), 108-127; doi: 10.1006/jcph.2001.6892.

[11] X. Zhang, C.-W. Shu, Positivity-preserving high order finite difference WENO schemes for compressible Euler equations, *J. of Comput. Physics*, **231**, No 5 (2012), 2245-2258; doi: 10.1016/j.jcp.2011.11.020.

[12] X. Cai, X. Zhang, J. Qiu, Positivity-preserving high order finite volume hweno schemes for compressible Euler equations, *J. of Scient. Computing*, **68**, No 2 (2016), 464-483; doi: 10.1007/s10915-015-0147-8.

[13] X. Hu, Q. Wang, N. Adams, An adaptive central-upwind weighted essentially non-oscillatory scheme, *J. of Comput. Physics*, **229**, No 23 (2010), 8952-8965; doi: 10.1016/j.jcp.2010.08.019.

[14] X. Hu, N. Adams, Scale separation for implicit large eddy simulation, *J. of Comput. Physics*, **230**, No 19 (2011), 7240-7249; doi: 10.1016/j.jcp.2011.05.023.

[15] X.Y. Hu, V.K. Tritschler, S. Pirozzoli, N.A. Adams, Dispersion-dissipation condition for finite difference schemes, *arXiv*: 1204.5088 (2012).

[16] L. Fu, X.Y. Hu, N.A. Adams, A family of high-order targeted ENO schemes for compressible-fluid simulations, *J. of Comput. Physics*, **305**, (2016), 333-359; doi: 10.1016/j.jcp.2015.10.037.

[17] F. Jia, Z. Gao, W.S. Don, A Spectral study on the dissipation and dispersion of the WENO schemes, *J. of Scient. Computing*, **63**, No 1 (2015), 49-77; doi: 10.1007/s10915-014-9886-1.

[18] M. Castro, B. Costa, W.S. Don, High order weighted essentially non-oscillatory WENO-Z schemes for hyperbolic conservation laws, *J. of Comput. Physics*, **230**, No 5 (2011), 1766-1792; doi: 10.1016/j.jcp.2010.11.028.

[19] L. Fu, X.Y. Hu, N.A. Adams, Targeted ENO schemes with tailored resolution property for hyperbolic conservation laws, *J. of Comput. Physics*, **349**, (2017), 97-121; doi: 10.1016/j.jcp.2017.07.054.

[20] W.-S. Don, R. Borges, Accuracy of the weighted essentially non-oscillatory conservative finite difference schemes, *J. of Comput. Physics*, **250** (2013), 347-372; doi: 10.1016/j.jcp.2013.05.018.

[21] S. Pirozzoli, On the spectral properties of shock-capturing schemes, *J. of Comput. Physics*, **219**, No 2 (2006), 489-497; doi: 10.1016/j.jcp.2006.07.009.

[22] V. Titarev, E. Toro, Finite-volume WENO schemes for three-dimensional conservation laws, *J. of Comput. Physics*, **201**, No 1 (2004), 238-260; doi: 10.1016/j.jcp.2004.05.015.

[23] E.F. Toro, The HLLC Riemann solver, *Shock Waves*, **29**, No 8 (2019), 1065-1082; doi: 10.1007/s00193-019-00912-4.

[24] C.-W. Shu, S. Osher, Efficient implementation of essentially non-oscillatory shock-capturing schemes, *J. of Comput. Physics*, **77**, No 2 (1988), 439-471; doi: 10.1016/0021-9991(88)90177-5.

[25] P.D. Lax, X.-D. Liu, Solution of two-dimensional riemann problems of gas dynamics by positive schemes, *SIAM J. on Scient. Computing*, **19**, No 2 (1998), 319-340; doi: 10.1137/S1064827595291819.

[26] P. Woodward, P. Colella, The numerical simulation of two-dimensional fluid flow with strong shocks, *J. of Comput. Physics*, **54**, No 1 (1984), 115-173; doi: 10.1016/0021-9991(84)90142-6.

[27] L. Fu, A low-dissipation finite-volume method based on a new TENO shock-capturing scheme, *Computer Phys. Communications*, **235**, (2019), 25-39; doi: 10.1016/j.cpc.2018.10.009.